SECTION EDITOR: JANEY L. WIGGS, MD, PhD

Cone Structure in Patients With Usher Syndrome Type III and Mutations in the *Clarin 1* Gene

Kavitha Ratnam, BS; Hanna Västinsalo, PhD; Austin Roorda, PhD; Eeva-Marja K. Sankila, MD, PhD; Jacque L. Duncan, MD

Objective: To study macular structure and function in patients with Usher syndrome type III (USH3) caused by mutations in the *Clarin 1* gene (*CLRN1*).

Methods: High-resolution macular images were obtained by adaptive optics scanning laser ophthalmoscopy and spectral domain optical coherence tomography in 3 patients with USH3 and were compared with those of age-similar control subjects. Vision function measures included best-corrected visual acuity, kinetic and static perimetry, and full-field electroretinography. Coding regions of the *CLRN1* gene were sequenced.

Results: *CLRN1* mutations were present in all the patients; a 20-year-old man showed compound heterozygous mutations (p.N48K and p.S188X), and 2 unrelated women aged 25 and 32 years had homozygous mutations (p.N48K). Best-corrected visual acuity ranged from 20/16 to 20/40, with scotomas beginning at 3° eccentricity. The inner segment–outer segment junction or the inner segment ellipsoid band was disrupted within 1° to 4° of the fovea, and the foveal inner and outer segment layers were significantly thinner than normal. Cones near the fovea in patients 1 and 2 showed normal spacing, and the preserved region ended abruptly. Retinal pigment epithelial cells were visible in patient 3 where cones were lost.

Conclusions: Cones were observed centrally but not in regions with scotomas, and retinal pigment epithelial cells were visible in regions without cones in patients with *CLRN1* mutations. High-resolution measures of retinal structure demonstrate patterns of cone loss associated with *CLRN1* mutations.

Clinical Relevance: These findings provide insight into the effect of *CLRN1* mutations on macular cone structure, which has implications for the development of treatments for USH3.

Trial Registration: clinicaltrials.gov Identifier: NCT00254605

JAMA Ophthalmol. 2013;131(1):67-74.
Published online September 10, 2012.
doi:10.1001/2013.jamaophthalmol.2

Author Affiliations:
Department of Ophthalmology, University of California, San Francisco, San Francisco (Ms Ratnam and Dr Duncan); Folkhälsan Institute of Genetics, Helsinki, Finland (Drs Västinsalo and Sankila); Department of Medical Genetics, University of Helsinki (Dr Västinsalo); School of Optometry, University of California, Berkeley, Berkeley; and Helsinki University Eye Hospital (Dr Sankila).

Usher syndrome (USH) is an autosomal recessive disease characterized by hearing loss, vestibular dysfunction, and retinitis pigmentosa.[1-3] Vision dysfunction includes early nyctalopia due to rod dysfunction, with secondary cone degeneration causing peripheral vision loss and eventual blindness. Usher syndrome is clinically and genetically heterogeneous. Of the 3 subtypes, USH type III (USH3; OMIM 276902) is distinguishable from types I and II by progressive, usually postlingual hearing loss and variable vestibular dysfunction, with the onset of vision symptoms varying but usually occurring by the second decade of life.[4-11] Although USH3 is the least common type of USH, it accounts for more than 40% of cases in Finnish and Ashkenazi Jewish populations.[8,9,12,13] Studies[8,12,14,15] have reported rod-cone degeneration with persistence of central cone function for decades and a rate of progression more rapid than that of USH2. Some patients have nonsyndromic retinitis pigmentosa with minimal hearing loss, whereas others have more severe hearing loss that can be mistaken for other USH subtypes; owing to the variable onset of ocular and auditory symptoms, USH3 is especially difficult to diagnose.[12,14,15]

The *USH3A* locus, chromosome 3q25.1, includes the *Clarin 1* gene (*CLRN1*; OMIM 606397).[1,4,14,16] The expression of *CLRN1* has been detected in the cochlea and retina by Northern blot analysis and reverse transcription–polymerase chain reaction.[4,16] To date, 17 mutations have been identified in the *CLRN1* gene, 15 causing USH3 and 2 missense mutations causing autosomal re-

©2013 American Medical Association. All rights reserved.
Downloaded From: http://archopht.jamanetwork.com/ by a University of California - Berkeley User on 08/07/2013

cessive retinitis pigmentosa.[17-20] In cell culture studies, wild-type CLRN1 protein is trafficked to the plasma membrane, and all the studied mutations cause abnormal protein localization and stability.[19] The most common North American mutation is c.144T→G (p.N48K), a mutation in codon 48 that causes the substitution of lysine for asparagine and disrupts the *N*-glycosylation consensus site.[12,21]

Although *CLRN1* gene expression has been localized to the ribbon synapses, inner segments (ISs), and cilia of mouse photoreceptors, the function of *CLRN1* in the human retina is unknown.[1,4,16,22-24] Given the phenotypic variability observed in patients with USH3, the effect of *CLRN1* mutations on cone structure in human eyes is not clearly understood. Although previous studies have used optical coherence tomography (OCT) and near-infrared reduced-illuminance autofluorescence imaging[14] to characterize patients with *CLRN1* mutations, no histologic studies of photoreceptors in human eyes have been published, to our knowledge.

Adaptive optics scanning laser ophthalmoscopy (AOSLO) uses adaptive optics to compensate for optical aberrations in living eyes, improving resolution of retinal images to a lateral resolution of approximately 2 μm.[25-30] Direct visualization of the cone mosaic in patients with retinal degenerations, combined with other imaging and diagnostic techniques, allows comparison of cone spacing with healthy individuals and can provide insight into the effects of different retinal degenerations on macular cones.[29-39] Herein we present high-resolution retinal images for 3 patients with USH3 with *CLRN1* mutations, allowing direct in vivo genotype-phenotype correlation of cone photoreceptor structure at the cellular level.

METHODS

The research procedures followed the tenets of the Declaration of Helsinki, and informed consent was obtained from all the participants. The study protocol was approved by the institutional review boards of the University of California, San Francisco; the University of California, Berkeley; and Helsinki University Eye Hospital.

CLINICAL EXAMINATION

Complete medical histories were obtained and medical records were reviewed, including onset of vision and hearing loss. Audiologic examinations included serial pure-tone audiometry and speech reception threshold testing. Best-corrected visual acuity was measured using a standard eye chart according to the Early Treatment of Diabetic Retinopathy Study protocol. Automated perimetry was completed using a Humphrey visual field analyzer (HFA II 750-6116-12.6; Carl Zeiss Meditec, Inc) 10-2 Swedish interactive threshold algorithm with measurement of foveal thresholds using a Goldmann III stimulus on a white background (31.5 apostilbs) and an exposure duration of 200 milliseconds. Goldmann kinetic perimetry was performed using V-4e and I-4e isopters, converted into retinal areas, and compared with the average V-4e and I-4e field areas for 10 eyes of 7 healthy individuals aged 20 to 35 years (3 women and 4 men; mean [SD] age, 24.1 [3.5] years); to account for the planimetric distortion of Goldmann perimetry, planar data were converted to solid visual field angles and retinal areas using previously published methods.[40] Pupils were dilated with a combination of tropicamide, 1%, and phenylephrine hydrochloride, 2.5%, before full-field electroretinography, which was performed after 45 minutes of dark adaptation using Burian-Allen contact lens electrodes (Hansen Ophthalmic Development Laboratory) according to International Society for Clinical Electrophysiology of Vision standards[41] and as described previously.[30] Amplitudes and timing with reference mean (SD) values are given in **Table 1**. Fundus-guided microperimetry (MP-1; Nidek Technologies America, Inc) was used to test 45 locations in the central 8° visual field, as previously described.[29,30,33] Numerical sensitivities in decibels were exported and superimposed on AOSLO images using MATLAB software (The MathWorks, Inc). The mean (SD) reference value across the central 10° for individuals aged 20 years was 19.9 (0.4) dB and for those aged 21 to 40 years was 19.5 (1.1) dB.[43]

Spectral domain OCT (SDOCT) and infrared SLO (Spectralis HRA + OCT laser scanning camera system; Heidelberg Engineering) were performed. The infrared beam of the super luminescent diode, center wavelength 870 nm, was used to acquire 20° horizontal scans; OCT images were averages of 100 B-scans through the fovea and averages of 10 B-scans for each location in the 20° × 15° volume image. Regions in which the IS ellipsoid (ISe) band[44] or the IS–outer segment (IS/OS) junction was intact were distinguished from regions where it was disrupted by visual inspection. Total foveal, outer nuclear layer, IS layer, and OS layer thicknesses were determined by manually analyzing SDOCT B-scans using the manufacturer's software and previously described methods.[45] Average thickness measurements were compared with those of 10 control subjects aged 16 to 28 years (6 females and 4 males; mean [SD] age, 23.3 [3.4] years) using a 2-tailed paired *t* test; $P < .05$ was considered significant.

GENETIC TESTING

Mutation analysis of the *CLRN1* gene was performed by sequencing the coding region. Genomic DNA was extracted from whole blood samples using genomic DNA purification kits (Puregene; Gentra Systems) or from saliva using DNA collection kits (Oragene; DNA Genotek, Inc). The 3 exons and the exon-intron boundaries of the *CLRN1* main splice variant (GenBank NM_174878) were screened for mutations by genomic sequencing, as previously described.[19]

AOSLO IMAGE ACQUISITION AND CONE SPACING ANALYSIS

High-resolution images were obtained using AOSLO of the eye, with better visual acuity for 3 patients with USH3 and 24 control subjects aged 14 to 37 years (11 females and 13 males; mean [SD] age, 23.3 [5.6] years). Images were processed to create montages of the macular region. Regions in which unambiguous cone mosaics were clearly visualized were selected for cone spacing measurements. The presence of cones in each region was further verified by visualization of the ISe band or the IS/OS junction in registered SDOCT scans. Customized software was used to determine quantitative cone spacing measures using previously described methods,[29,30,33,46] and AOSLO cone spacing data have been shown to match well with histologic data.[29] Cone spacing measurements for the patients were compared with those for the 24 control subjects. An exponential function was fit to the spacing data:

$$\text{Cone Spacing} = Ae^{(-C \times \text{eccentricity})} + B$$

where *A*, *B*, and *C* are constants. Cone locations were measured as eccentricity in degrees relative to the anatomical fovea, defined as the base of the foveal pit as visualized on SDOCT im-

©2013 American Medical Association. All rights reserved.
Downloaded From: http://archopht.jamanetwork.com/ by a University of California - Berkeley User on 08/07/2013

Table 1. Summary of Retinal Functional and Structural Testing

Patient No./ Sex/ Age, y	*CLRN1* Mutations	Eye	Ages at Onset, Vision (v) and Hearing (h) Loss, y; SRT (Age, y)	Symptomatic Disease Duration, y[a]	BCVA; ETDRS Score[b]; Foveal Threshold, dB	ffERG Photopic 30-Hz Flicker Amplitude and Timing[c]	Fundus-Guided Microperimetry	Automated Perimetry, Humphrey Visual Field	Kinetic Perimetry, Goldmann Visual Field	Preserved Visual Field Areas, %[d]	
										I-4e	V-4e
1/M/20	Compound heterozygous c.144T>G (p.N48K) and c.563C>A (p.S188X)	OS	(v) 13, (h) 3; RE 66 dB, LE 77 dB (17)	7	20/16; 90; 36	3.5 μV and 32.5 msec	Normal sensitivity in central 4° and reduced by 2-4 dB peripherally except for severely reduced region superiorly	Visual field constricted to central 7°	Pericentral scotoma from 20° to 45°	0.6	32.1
2/F/25	Homozygous c.144T>G	OD	(v) 18, (h) 13; RE 40 dB, LE 40 dB (23)	7	20/20; 85; 35	3.6 μV and 30 msec	Normal sensitivity in all tested locations	Reduced peripheral sensitivity	Incomplete pericentral scotoma from 25° to 50°	5.5	58.2
3/F/32	Homozygous c.144T>G	OS	(v) 12, (h) 13; RE 35 dB, LE 35 dB (16)	20	20/40; 70; 34	Not measureable	Sensitivity reduced 5-15 dB in central preserved region and ≥15 dB 3° from fovea	Visual field constricted to central 8° with nonhomogeneous sensitivity loss extending into fixation	Central 18°-diameter island with preserved temporal crescent from 135° to 225°	1.0	12.2

Abbreviations: BCVA, best-corrected visual acuity; ETDRS, Early Treatment of Diabetic Retinopathy Study; ffERG, full-field electroretinogram; LE, left ear; msec, milliseconds; RE, right ear; SRT (Age, y), speech reception thresholds and age at time of most recent SRT testing (SRT reference range, 0-5 dB).

[a] Symptomatic disease duration is defined as age at examination minus age at onset of vision loss in years.[42]

[b] The ETDRS visual acuity scores are expressed as the number of letters correctly identified.

[c] Mean reference ffERG amplitudes: rod, 272 μV, cone flicker, 121 μV; 2 SD below normal is 95 μV for rod b-wave and 56 μV for cone flicker; normal cone flicker timing is less than 32 msec.

[d] Preserved visual field areas are expressed as a percentage of the average field area for 7 control subjects aged 20 to 35 years (mean [SD] age, 24.1 [3.5] years).

ages, and cone spacing in patients was measured at a range of eccentricities in which unambiguous cone mosaics were observed. The 95% CIs were estimated using the MATLAB curve-fitting toolbox (The Mathworks, Inc). *z* Scores were computed as the number of standard deviations from the mean reference cone spacing at the eccentricity measured. *z* Scores between –2 and 2 (±SD) were considered within the reference range.

To determine fixational stability and proximity to the anatomical fovea, the location of the retina used for fixation (preferred retinal locus) was determined by recording a video while the patient looked at a target that was provided through modulation of the AOSLO scanning raster.[47] As such, the fixation target was encoded directly into the video, and the region of the retina used to fixate the target was determined using custom image analysis tools written in MATLAB.

RESULTS

The clinical characteristics of the patients are summarized in Table 1. Three unrelated patients with USH3 ranged from 20 to 32 years old. Mutation analysis of *CLRN1* in patient 1 revealed compound heterozygous mutations: p.N48K and p.S188X, a novel C>A change at nucleotide position c.563 predicted to result in an early termination signal at codon 188. Patients 2 and 3 showed homozygous p.N48K mutations in *CLRN1*. Best-corrected visual acuity ranged from 20/16 to 20/40. Small central posterior subcapsular cataracts were present in patient 3 only. All the patients reported progressive sensorineural hearing loss. Serial audiograms performed between ages 4 and 23 demonstrated moderate to severe hearing loss, with a U-shaped audiogram in patients 1 and 3, whereas patient 2 had moderate hearing loss with a down-sloping audiogram and elevated hearing thresholds, especially at high frequencies. All 3 patients showed elevated speech reception thresholds (reference range, 0-5 dB) (Table 1).

Foveal sensitivities in patients ranged from 34 to 36 dB. Full-field electroretinography in all the patients showed severe outer retinal dysfunction affecting rods to a greater extent than cones; rod-mediated responses were reduced below levels that can be measured reliably for all the patients. Cone electroretinographic responses were severely reduced but measurable in patients 1 and 2 but unmeasurable in patient 3 (Table 1). Goldmann I-4e and V-4e visual field areas were severely reduced in all 3 patients but were best preserved in patient 2 (5.5% and 58.2% of normal for the I-4e and V-4e targets, respectively) (**Figure 1** and Table 1). Automated perimetry showed scotomas beginning 3° to 8° from fixation (Figure 1). Sensitivity was preserved and within the reference range throughout much of the central 4° in patient 1 but was reduced by greater than 1 log unit superiorly where unambiguous cones were not visualized and by 2 to 4 dB at greater eccentricities (Figure 1). Sensitivity was within the reference range at all locations in the central 4° in patient 2. In patient 3, sensitivity was reduced by 5 to 10 dB in the central preserved region and by at least 20 dB beginning 3° from the fovea (Figure 1).

Total foveal and outer nuclear layer thicknesses in patient 1 were greater than the reference values, whereas the IS and OS layers were significantly thinner (**Table 2**). Patient 2 had total foveal and outer nuclear layer thicknesses within the reference range but significantly thinner IS and

©2013 American Medical Association. All rights reserved.
Downloaded From: http://archopht.jamanetwork.com/ by a University of California - Berkeley User on 08/07/2013

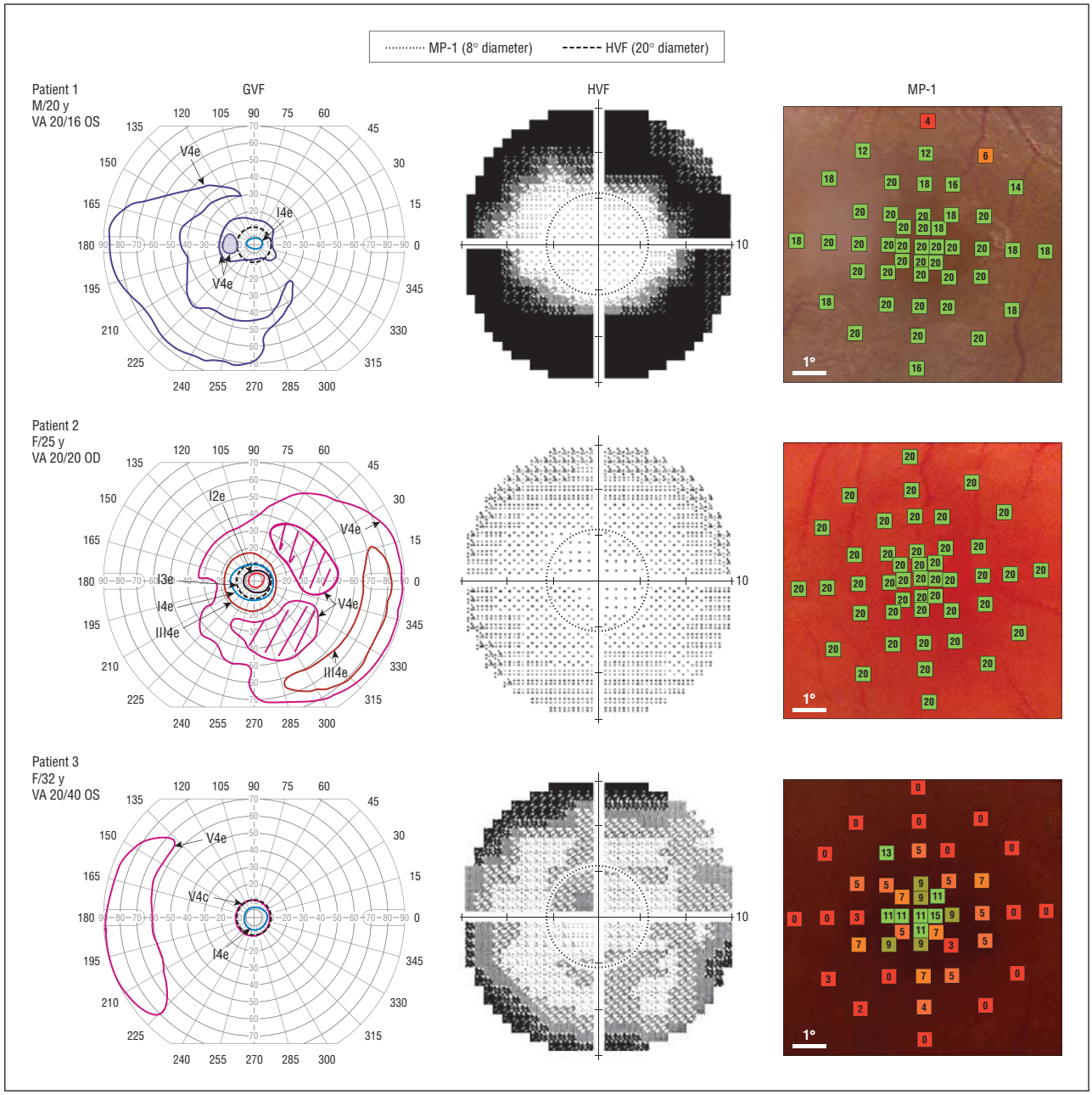

Figure 1. Visual field loss in 3 patients with Usher syndrome type III. Goldmann (GVF) and Humphrey (HVF) visual fields showed peripheral scotomas. Fundus-guided microperimetry (MP-1) showed reduced sensitivity in the central 8° (green indicates normal; and red and orange, reduced sensitivity). VA indicates visual acuity.

OS layers, and patient 3′s total foveal, outer nuclear layer, IS layer, and OS layer were significantly thinner than the reference values (Table 2). Disruption of the ISe band or the IS/OS junction on SDOCT was present beginning 4° from fixation in patients 1 and 2 and 1° in patient 3 (**Figure 2**). All the patients retained fixation near or at the anatomical fovea (**Figure 3**). Fixation was least stable in patient 3, whose AOSLO image revealed sparse cones near the preferred retinal locus (Figure 3). In patients 1 and 2, cones within 4° of the fovea had normal spacing (z scores within ± 2), but the central preserved region ended abruptly, and peripheral photoreceptor degeneration precluded accurate cone-spacing measures (Figure 3; the SDOCT scan is 1° eccentric from the fovea for patient 2 to compare 2 regions of varying reflectance of the ISe band with the corresponding AOSLO locations). In patient 3, who had the most advanced disease, retinal pigment epithelial (RPE) cells were seen throughout the macular region (Figure 3). In some regions, the cone mosaic was visible, but without normal contrast and packing regularity; quantitative measures of cone spacing were not possible. Cone spacing in patients 1 and 2 was within the 95% CIs around the mean reference value, indicating that significant cone loss had not occurred at locations where cones were visualized (**Figure 4**).

COMMENT

The present study demonstrates cone photoreceptor abnormalities in patients with *CLRN1* mutations and vary-

©2013 American Medical Association. All rights reserved.
Downloaded From: http://archopht.jamanetwork.com/ by a University of California - Berkeley User on 08/07/2013

Table 2. Spectral Domain Optical Coherence Tomography Foveal Thicknesses

Patient No./Sex/ Age, y	*CLRN1* Mutations	Eye	Foveal Thicknesses, Mean (SD), μm[a]			
			Total	ONL	IS Layer	OS Layer
1/M/20	Compound heterozygous c.144T>G (p.N48K) and c.563C>A (p.S188X)	OS	248.2 (0.8)	133.8 (0.8)	32.2 (0.4)	45.8 (0.8)
P value			<.001	<.001	<.001	<.001
2/F/25	Homozygous c.144T>G	OD	226.8 (0.8)	106.6 (0.5)	28.8 (0.4)	49.8 (0.8)
P value			.48	.09	<.001	.002
3/F/32	Homozygous c.144T>G	OS	119.8 (0.8)	43.4 (0.5)	23.2 (0.4)	24.8 (0.8)
P value			<.001	<.001	<.001	<.001
	Mean reference values[b]		228.2 (13.4)	109.1 (9.9)	34.2 (2.0)	52.3 (4.5)

Abbreviations: IS, inner segment; ONL, outer nuclear layer; OS, outer segment.
[a] Thickness values represent the average of 5 measures within 1° of the fovea.
[b] Control subjects included 6 females and 4 males aged 16 to 28 years (mean [SD] age, 23.3 [3.4] years).

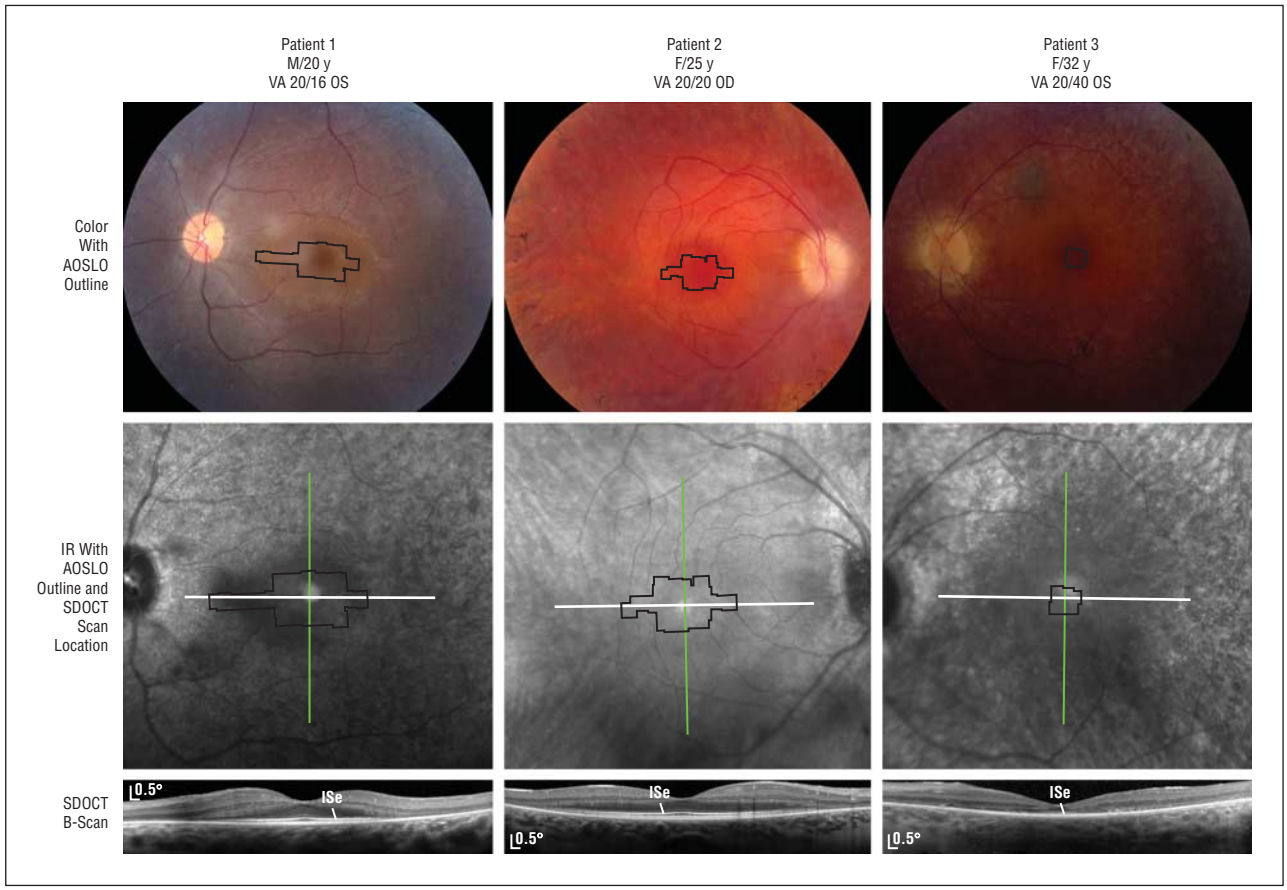

Figure 2. Fundus and spectral domain optical coherence tomography (SDOCT) images in 3 patients with Usher syndrome type III. Black outlines indicate areas imaged by adaptive optics scanning laser ophthalmoscopy (AOSLO); and white lines, SDOCT scans. The inner segment ellipsoid (ISe) was disrupted for all the patients and correlated with lack of visible cone mosaics in AOSLO images. IR indicates infrared; and VA, visual acuity.

ing degrees of disease severity. Herein, preserved vision correlated with regions where the ISe band or the IS/OS junction was intact and unambiguous cone mosaics showed normal cone spacing (Figures 3 and 4). The observation of normal cone spacing where cones were visualized in patients with *CLRN1* mutations distinguishes retinal degeneration due to *CLRN1* mutations from retinal degeneration caused by mutations in other genes that cause cone spacing abnormalities throughout the macula, including *rhodopsin*,[29,36] *RPGR*,[29] *RDS*,[37] *ABCA4*,[38] and *ATPase6*.[30] In regions in which vision was abnormal, the ISe band or the IS/OS junction was disrupted, unambiguous cone mosaics were not seen, and cone reflectivity was reduced. In patient 3, AOSLO images revealed RPE structure in regions where distinct cone mosaics were not visualized; the presence of an intact RPE layer on SDOCT scans suggests that RPE cells persist in the absence of cones (Figures 2 and 3). Lack of visible cone mosaics in the AOSLO image may be due to abnormal waveguiding properties in cones with abnormal OSs

©2013 American Medical Association. All rights reserved.
Downloaded From: http://archopht.jamanetwork.com/ by a University of California - Berkeley User on 08/07/2013

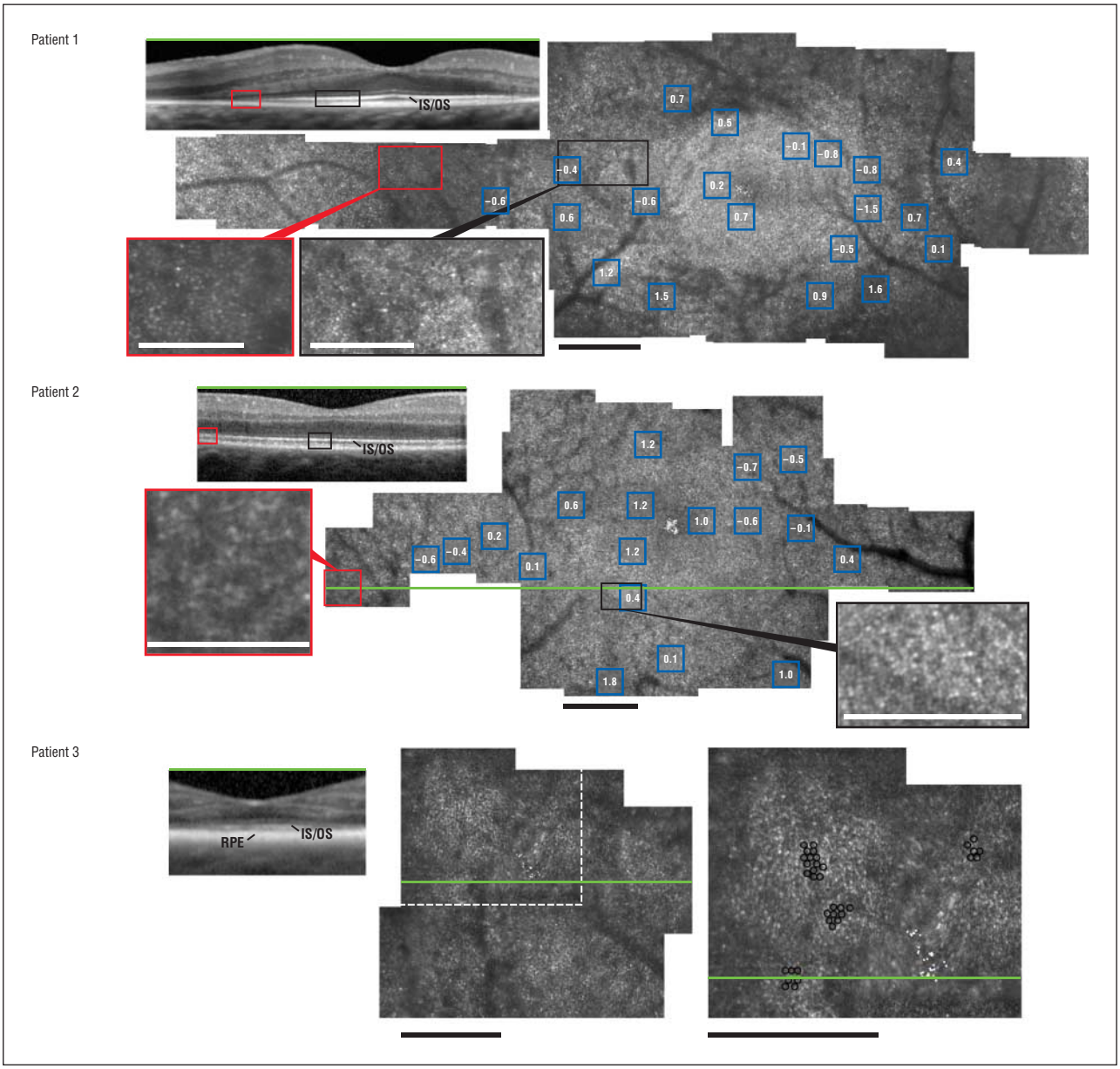

Figure 3. High-resolution images for 3 patients with Usher syndrome type III show reduced cones and inner segment ellipsoid disruption (red boxes). Green lines indicate spectral domain optical coherence tomography B-scans; white dots, fixation; blue boxes, cone spacing *z* scores; and black circles, individual retinal epithelial pigment (RPE) cells. Scale bars represent 1° (black) and 0.5° (white). IS indicates inner segment; OS, outer segment.

or photoreceptor loss; the direct observation of RPE cells in eyes with cone photoreceptor loss has been described.[33] Previous studies of *CLRN1* mutations used near-infrared reduced-illuminance autofluorescence imaging to estimate RPE health and melanin integrity in patients with USH3 and demonstrated loss of RPE melanin parafoveally but preserved melanin centrally.[14] The visibility of RPE mosaics near the fovea in patient 3 suggests that photoreceptor loss may precede RPE atrophy in the progression of USH3, although AOSLO does not provide information on the health of these RPE cells. Sparse cones were likely present since SDOCT scans showed that the ISe band or the IS/OS junction was preserved near the fovea in patient 3, which likely mediate the patient's foveal fixation, with reduced visual acuity and sensitivity in areas with visible RPE cells (Figure 3).

Other studies[14] have reported that central cone function declines slowly in patients with *CLRN1* mutations, persisting for decades. The 3 patients in the present study had variable degrees of disease severity and peripheral cone loss, but the better-seeing eye of all the patients had visual acuity of at least 20/40 and near-normal foveal sensitivities (34-36 dB). Patient 3 retained foveal fixation and visual acuity of 20/40 despite disruption of the ISe band or IS/OS junction on SDOCT scans and lack of visible cone mosaics in AOSLO images. These observations suggest that traditional measures of vision, such as acuity, are inadequate for measuring disease severity, and more sensitive mechanisms for observing macular structure, such as SDOCT and AOSLO, are important for monitoring disease severity and progression. In addition, future studies incorporating individual cell stimulus delivery

©2013 American Medical Association. All rights reserved.
Downloaded From: http://archopht.jamanetwork.com/ by a University of California - Berkeley User on 08/07/2013

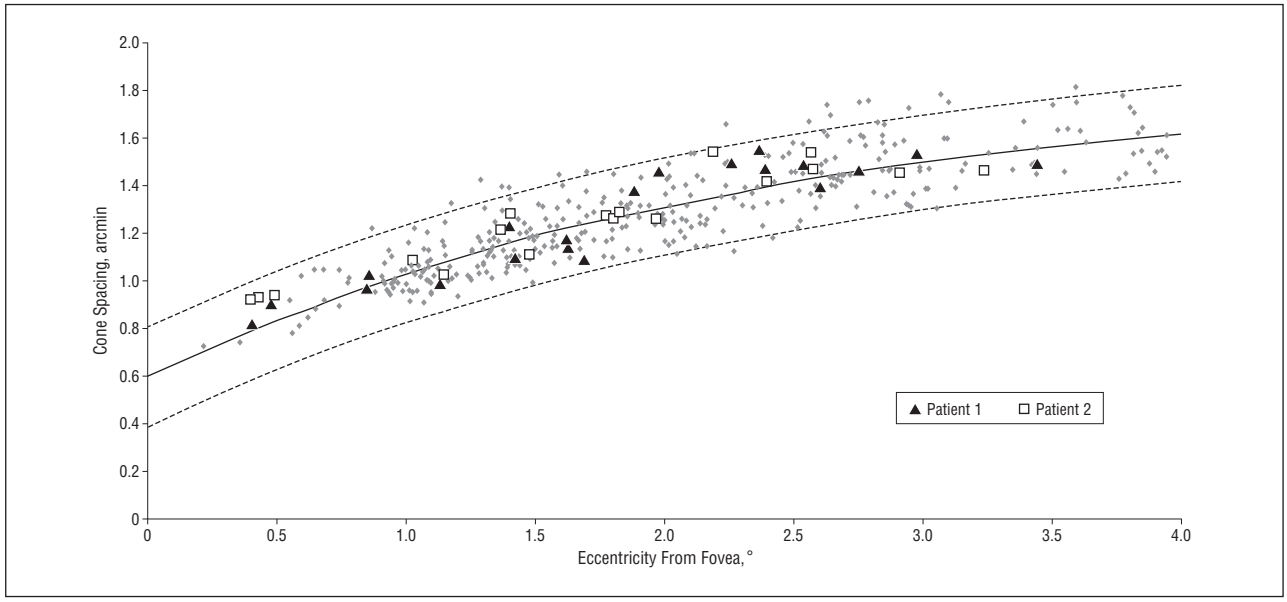

Figure 4. Cone spacing vs distance from fovea. Cone spacing measurements on adaptive optics scanning laser ophthalmoscopy in patients 1 and 2 were compared with those from 24 control subjects (gray dots). Solid black line indicates mean reference values; and dashed lines, 95% CIs.

using AOSLO may provide more sensitive high-resolution measures of cone structure and function in patients with USH3.[48]

Although the present study did not include longitudinal observation, studying 3 patients with USH3 with varying degrees of disease severity allowed comparison of clinical measures at different stages of disease progression. Given the variability in age at onset, the duration of symptomatic disease provides a better indication of disease status than does chronological age.[42,49,50] Although patients 1 and 2 had similar symptomatic disease durations, patient 1 showed more severe visual field constriction (Figure 1) despite increased retinal thickness at the fovea (Table 2). Increased foveal thickness may be caused by retinal remodeling, cystoid macular edema, epiretinal membrane formation, or subretinal fluid; the SDOCT images in patient 1 showed no macular edema, epiretinal membrane, or subretinal fluid (Figure 2), perhaps indicating that the increased foveal thickness is due to retinal remodeling.[51-54] Alternatively, the increased foveal thickness in patient 1 may be sex related. Various studies[55-60] have observed significantly greater central macular thickness in males (by 10-22 μm) than in females, although other studies[61-63] have shown no significant difference. As degeneration progresses, the retina thins with photoreceptor loss, resulting in reduced retinal and outer retinal layer thickness, as observed in patient 3 (Table 2).

Foveal preservation may make USH3-associated retinal degeneration a suitable candidate for treatment with neuroprotective drugs designed to slow disease progression.[36,64] However, since foveal cones are relatively preserved, clinical trials designed to measure efficacy of experimental therapies should include additional outcome measures, including fundus-guided microperimetry, and high-resolution structural measures, such as OCT and AOSLO, to measure safety and efficacy with greater sensitivity than is provided by traditional measures, such as visual acuity.

In conclusion, AOSLO and SDOCT of patients with USH3 with *CLRN1* mutations provided high-resolution images of the central retina and demonstrated the effects of *CLRN1* mutations on photoreceptor structure. Continuing analyses of retinal structure and function on a scale such as the measures presented may provide additional insight into the effects of *CLRN1* mutations on macular photoreceptors in patients with USH3.

Submitted for Publication: April 25, 2012; accepted June 12, 2012.
Published Online: September 10, 2012. doi:10.1001/2013.jamaophthalmol.2
Correspondence: Jacque L. Duncan, MD, Beckman Vision Center, University of California, San Francisco, School of Medicine, 10 Koret Way, Room K-129, San Francisco, CA 94143-0730.
Financial Disclosure: Dr Roorda holds a patent (US patent 7118216) for AOSLO technology in conjunction with the University of Houston and the University of Rochester.
Funding/Support: This study was supported by a Physician Scientist Award and an unrestricted grant from Research to Prevent Blindness (Dr Duncan); a clinical center grant from the Foundation Fighting Blindness (Drs Roorda and Duncan); grants EY002162 (Dr Duncan) and EY014375 (Dr Roorda) from the National Eye Institute, National Institutes of Health; That Man May See, Inc (Dr Duncan); the Bernard A. Newcomb Macular Degeneration Fund (Dr Duncan); Hope for Vision (Dr Duncan); De Blindas Vänner Foundation; the Eye and Tissue Bank Foundation (Finland) (Dr Västinsalo); and the Usher III Initiative (Drs Västinsalo and Sankila).

REFERENCES

1. Fields RR, Zhou G, Huang D, et al. Usher syndrome type III: revised genomic structure of the USH3 gene and identification of novel mutations. *Am J Hum Genet.* 2002;71(3):607-617.

©2013 American Medical Association. All rights reserved.
Downloaded From: http://archopht.jamanetwork.com/ by a University of California - Berkeley User on 08/07/2013

2. Kimberling WJ, Möller C. Clinical and molecular genetics of Usher syndrome. *J Am Acad Audiol*. 1995;6(1):63-72.
3. Millan JM, Aller E, Jaijo T, Blanco-Kelly F, Gimenez-Pardo A, Ayuso C. An update on the genetics of Usher syndrome. *J Ophthalmol*. doi:10.115/2011/417217.
4. Joensuu T, Hämäläinen R, Yuan B, et al. Mutations in a novel gene with transmembrane domains underlie Usher syndrome type 3. *Am J Hum Genet*. 2001; 69(4):673-684.
5. Cohen M, Bitner-Glindzicz M, Luxon L. The changing face of Usher syndrome: clinical implications. *Int J Audiol*. 2007;46(2):82-93.
6. Kumar A, Fishman G, Torok N. Vestibular and auditory function in Usher's syndrome. *Ann Otol Rhinol Laryngol*. 1984;93(6, pt 1):600-608.
7. Pennings RJ, Fields RR, Huygen PL, Deutman AF, Kimberling WJ, Cremers CW. Usher syndrome type III can mimic other types of Usher syndrome. *Ann Otol Rhinol Laryngol*. 2003;112(6):525-530.
8. Pakarinen L, Karjalainen S, Simola KO, Laippala P, Kaitalo H. Usher's syndrome type 3 in Finland. *Laryngoscope*. 1995;105(6):613-617.
9. Karjalainen S, Pakarinen L, Teräsvirta M, Kääriäinen H, Vartiainen E. Progressive hearing loss in Usher's syndrome. *Ann Otol Rhinol Laryngol*. 1989;98 (11):863-866.
10. Smith RJ, Berlin CI, Hejtmancik JF, et al; Usher Syndrome Consortium. Clinical diagnosis of the Usher syndromes. *Am J Med Genet*. 1994;50(1):32-38.
11. Pennings RJ, Kremer H, Deutman AF, Kimberling WJ, Cremers CW. From gene to disease: genetic causes of hearing loss and visual impairment sometimes accompanied by vestibular problems (Usher syndrome). *Ned Tijdschr Geneeskd*. 2002;146(49):2354-2358.
12. Ness SL, Ben-Yosef T, Bar-Lev A, et al. Genetic homogeneity and phenotypic variability among Ashkenazi Jews with Usher syndrome type III. *J Med Genet*. 2003; 40(10):767-772.
13. Joensuu T, Hämäläinen R, Lehesjoki AE, de la Chapelle A, Sankila EM. A sequence-ready map of the Usher syndrome type III critical region on chromosome 3q. *Genomics*. 2000;63(3):409-416.
14. Herrera W, Aleman TS, Cideciyan AV, et al. Retinal disease in Usher syndrome III caused by mutations in the clarin-1 gene. *Invest Ophthalmol Vis Sci*. 2008; 49(6):2651-2660.
15. Plantinga RF, Pennings RJ, Huygen PL, et al. Visual impairment in Finnish Usher syndrome type III. *Acta Ophthalmol Scand*. 2006;84(1):36-41.
16. Adato A, Vreugde S, Joensuu T, et al. USH3A transcripts encode clarin-1, a four-transmembrane-domain protein with a possible role in sensory synapses. *Eur J Hum Genet*. 2002;10(6):339-350.
17. Akoury E, El Zir E, Mansour A, Mégarbané A, Majewski J, Slim R. A novel 5-bp deletion in Clarin 1 in a family with Usher syndrome. *Ophthalmic Genet*. 2011; 32(4):245-249.
18. Dreyer B, Brox V, Tranebjaerg L, et al. Spectrum of USH2A mutations in Scandinavian patients with Usher syndrome type II. *Hum Mutat*. 2008;29(3):451.
19. Isosomppi J, Västinsalo H, Geller SF, Heon E, Flannery JG, Sankila EM. Disease-causing mutations in the CLRN1 gene alter normal CLRN1 protein trafficking to the plasma membrane. *Mol Vis*. 2009;15:1806-1818.
20. Khan MI, Kersten FF, Azam M, et al. *CLRN1* mutations cause nonsyndromic retinitis pigmentosa. *Ophthalmology*. 2011;118(7):1444-1448.
21. Tian G, Zhou Y, Hajkova D, et al. Clarin-1, encoded by the Usher syndrome III causative gene, forms a membranous microdomain: possible role of clarin-1 in organizing the actin cytoskeleton. *J Biol Chem*. 2009;284(28):18980-18993.
22. Zallocchi M, Meehan DT, Delimont D, et al. Localization and expression of clarin-1, the *Clrn1* gene product, in auditory hair cells and photoreceptors. *Hear Res*. 2009;255(1-2):109-120.
23. Ebermann I, Scholl HP, Charbel Issa P, et al. A novel gene for Usher syndrome type 2: mutations in the long isoform of whirlin are associated with retinitis pigmentosa and sensorineural hearing loss. *Hum Genet*. 2007;121(2):203-211.
24. Västinsalo H, Jalkanen R, Dinculescu A, et al. Alternative splice variants of the USH3A gene Clarin 1 (*CLRN1*). *Eur J Hum Genet*. 2011;19(1):30-35.
25. Romero-Borja F, Venkateswaran K, Roorda A, Hebert T. Optical slicing of human retinal tissue in vivo with the adaptive optics scanning laser ophthalmoscope. *Appl Opt*. 2005;44(19):4032-4040.
26. Roorda A, Williams DR. Optical fiber properties of individual human cones. *J Vis*. 2002;2(5):404-412.
27. Zhang Y, Roorda A. Evaluating the lateral resolution of the adaptive optics scanning laser ophthalmoscope. *J Biomed Opt*. 2006;11(1):014002.
28. Zhang Y, Poonja S, Roorda A. MEMS-based adaptive optics scanning laser ophthalmoscopy. *Opt Lett*. 2006;31(9):1268-1270.
29. Duncan JL, Zhang Y, Gandhi J, et al. High-resolution imaging with adaptive optics in patients with inherited retinal degeneration. *Invest Ophthalmol Vis Sci*. 2007;48(7):3283-3291.
30. Yoon MK, Roorda A, Zhang Y, et al. Adaptive optics scanning laser ophthalmoscopy images in a family with the mitochondrial DNA T8993C mutation. *Invest Ophthalmol Vis Sci*. 2009;50(4):1838-1847.
31. Godara P, Rha J, Tait DM, et al. Unusual adaptive optics findings in a patient with bilateral maculopathy. *Arch Ophthalmol*. 2010;128(2):253-254.
32. Rha J, Dubis AM, Wagner-Schuman M, et al. Spectral domain optical coherence tomography and adaptive optics: imaging photoreceptor layer morphology to interpret preclinical phenotypes. *Adv Exp Med Biol*. 2010;664:309-316.
33. Roorda A, Zhang Y, Duncan JL. High-resolution in vivo imaging of the RPE mosaic in eyes with retinal disease. *Invest Ophthalmol Vis Sci*. 2007;48(5):2297-2303.
34. Wolfing JI, Chung M, Carroll J, Roorda A, Williams DR. High-resolution retinal imaging of cone-rod dystrophy. *Ophthalmology*. 2006;113(6):1019.
35. Choi SS, Doble N, Hardy JL, et al. In vivo imaging of the photoreceptor mosaic in retinal dystrophies and correlations with visual function. *Invest Ophthalmol Vis Sci*. 2006;47(5):2080-2092.
36. Talcott KE, Ratnam K, Sundquist SM, et al. Longitudinal study of cone photoreceptors during retinal degeneration and in response to ciliary neurotrophic factor treatment. *Invest Ophthalmol Vis Sci*. 2011;52(5):2219-2226.
37. Duncan JL, Talcott KE, Ratnam K, et al. Cone structure in retinal degeneration associated with mutations in the peripherin/RDS gene. *Invest Ophthalmol Vis Sci*. 2011;52(3):1557-1566.
38. Chen Y, Ratnam K, Sundquist SM, et al. Cone photoreceptor abnormalities correlate with vision loss in patients with Stargardt disease. *Invest Ophthalmol Vis Sci*. 2011;52(6):3281-3292.
39. Ooto S, Hangai M, Takayama K, et al. High-resolution photoreceptor imaging in idiopathic macular telangiectasia type 2 using adaptive optics scanning laser ophthalmoscopy. *Invest Ophthalmol Vis Sci*. 2011;52(8):5541-5550.
40. Dagnelie G. Conversion of planimetric visual field data into solid angles and retinal areas. *Clin Vis Sci*. 1990;5(1):95-100.
41. Marmor MF, Holder GE, Seeliger MW, Yamamoto S; International Society for Clinical Electrophysiology of Vision. Standard for clinical electroretinography (2004 update). *Doc Ophthalmol*. 2004;108(2):107-114.
42. Iannaccone A, Kritchevsky SB, Ciccarelli ML, et al. Kinetics of visual field loss in Usher syndrome type II. *Invest Ophthalmol Vis Sci*. 2004;45(3):784-792.
43. Midena E, Cavarzeran F; Microperimetry Study Group. Normal age-related values for fundus-related perimetry (microperimetry) with MP1 microperimeter [ARVO E-Abstract 1672]. Presented at: 2011 Annual Meeting of the Association for Research in Vision and Ophthalmology; May 4, 2011; Fort Lauderdale, Florida.
44. Spaide RF, Curcio CA. Anatomical correlates to the bands seen in the outer retina by optical coherence tomography: literature review and model. *Retina*. 2011; 31(8):1609-1619.
45. Duncan JL, Ratnam K, Birch DG, et al. Abnormal cone structure in foveal schisis cavities in X-linked retinoschisis from mutations in exon 6 of the *RS1* gene. *Invest Ophthalmol Vis Sci*. 2011;52(13):9614-9623.
46. Roorda A, Metha AB, Lennie P, Williams DR. Packing arrangement of the three cone classes in primate retina. *Vision Res*. 2001;41(10-11):1291-1306.
47. Poonja S, Patel S, Henry L, Roorda A. Dynamic visual stimulus presentation in an adaptive optics scanning laser ophthalmoscope. *J Refract Surg*. 2005;21 (5):S575-S580.
48. Tuten WS, Tiruveedhula P, Roorda A. Adaptive optics scanning laser ophthalmoscope-based microperimetry. *Optom Vis Sci*. 2012;89(5):563-574.
49. Massof R, Dagnelie G, Benzschawel T, Palmer R, Finkelstein D. First order dynamics of visual field loss in retinitis pigmentosa. *Clin Vis Sci*. 1990;5:1-26.
50. Fishman GA, Bozbeyoglu S, Massof RW, Kimberling WJ. Natural course of visual field loss in patients with type 2 Usher syndrome. *Retina*. 2007;27(5): 601-608.
51. Marc RE. Injury and repair: retinal remodeling. In: Dartt DA, ed. *Encyclopedia of the Eye*. Vol 2. Amsterdam, the Netherlands: Elsevier/Academic Press; 2010: 414-420.
52. Marc RE, Jones BW. Retinal remodeling in inherited photoreceptor degenerations. *Mol Neurobiol*. 2003;28(2):139-147.
53. Jones BW, Marc RE. Retinal remodeling during retinal degeneration. *Exp Eye Res*. 2005;81(2):123-137.
54. Jacobson SG, Cideciyan AV, Sumaroka A, et al. Remodeling of the human retina in choroideremia: rab escort protein 1 (*REP-1*) mutations. *Invest Ophthalmol Vis Sci*. 2006;47(9):4113-4120.
55. Adhi M, Aziz S, Muhammad K, Adhi MI. Macular thickness by age and gender in healthy eyes using spectral domain optical coherence tomography. *PLoS One*. 2012;7(5):e37638.
56. Song WK, Lee SC, Lee ES, Kim CY, Kim SS. Macular thickness variations with sex, age, and axial length in healthy subjects: a spectral domain-optical coherence tomography study. *Invest Ophthalmol Vis Sci*. 2010;51(8):3913-3918.
57. Kelty PJ, Payne JF, Trivedi RH, Kelty J, Bowie EM, Burger BM. Macular thickness assessment in healthy eyes based on ethnicity using Stratus OCT optical coherence tomography. *Invest Ophthalmol Vis Sci*. 2008;49(6):2668-2672.
58. Wagner-Schuman M, Dubis AM, Nordgren RN, et al. Race- and sex-related differences in retinal thickness and foveal pit morphology. *Invest Ophthalmol Vis Sci*. 2011;52(1):625-634.
59. Massin P, Erginay A, Haouchine B, Mehidi AB, Paques M, Gaudric A. Retinal thickness in healthy and diabetic subjects measured using optical coherence tomography mapping software. *Eur J Ophthalmol*. 2002;12(2):102-108.
60. Wong AC, Chan CW, Hui SP. Relationship of gender, body mass index, and axial length with central retinal thickness using optical coherence tomography. *Eye (Lond)*. 2005;19(3):292-297.
61. Sull AC, Vuong LN, Price LL, et al. Comparison of spectral/Fourier domain optical coherence tomography instruments for assessment of normal macular thickness. *Retina*. 2010;30(2):235-245.
62. Chan A, Duker JS, Ko TH, Fujimoto JG, Schuman JS. Normal macular thickness measurements in healthy eyes using Stratus optical coherence tomography. *Arch Ophthalmol*. 2006;124(2):193-198.
63. Grover S, Murthy RK, Brar VS, Chalam KV. Normative data for macular thickness by high-definition spectral-domain optical coherence tomography (spectralis). *Am J Ophthalmol*. 2009;148(2):266-271.
64. Sieving PA, Caruso RC, Tao W, et al. Ciliary neurotrophic factor (CNTF) for human retinal degeneration: phase I trial of CNTF delivered by encapsulated cell intraocular implants. *Proc Natl Acad Sci U S A*. 2006;103(10):3896-3901.

©2013 American Medical Association. All rights reserved.

Downloaded From: http://archopht.jamanetwork.com/ by a University of California - Berkeley User on 08/07/2013